


High-Resolution Coherent Probe Spectroscopy of a Polariton Quantum Fluid

F. Claude,¹ M. J. Jacquet¹, R. Usciati², I. Carusotto², E. Giacobino,¹ A. Bramati¹ and Q. Glorieux¹

¹Laboratoire Kastler Brossel, Sorbonne Université, ENS-Université PSL, Collège de France, CNRS, 4 place Jussieu, 75252 Paris Cedex 05, France

²INO-CNR BEC Center and Dipartimento di Fisica, Università di Trento, via Sommarive 14, I-38123 Trento, Italy

 (Received 18 December 2021; revised 29 April 2022; accepted 8 August 2022; published 29 August 2022)

Characterizing elementary excitations in quantum fluids is essential to study their collective effects. We present an original angle-resolved coherent probe spectroscopy technique to study the dispersion of these excitation modes in a fluid of polaritons under resonant pumping. Thanks to the unprecedented spectral and spatial resolution, we observe directly the low-energy phononic behavior and detect the negative-energy modes, i.e., the *ghost branch*, of the dispersion relation. In addition, we reveal narrow spectral features precursory of dynamical instabilities due to the intrinsic out-of-equilibrium nature of the system. This technique provides the missing tool for the quantitative study of quantum hydrodynamics in polariton fluids.

DOI: [10.1103/PhysRevLett.129.103601](https://doi.org/10.1103/PhysRevLett.129.103601)

The phenomenology of superfluids and Bose-Einstein condensates is generally understood in terms of quantum hydrodynamics. From liquid helium to ultracold atoms, these hydrodynamic properties depend on the dispersion of the collective excitation modes in the quantum fluid, which, in the dilute regime, are described by the Bogoliubov theory [1–4]. The Bogoliubov dispersion has a linear dependence on the wave number (k) at low wave number, where excitations are phonons (long-wavelength collective modes of the fluid), and a quadratic dependence at high wave number, where excitations behave like free particles [3,5–9]. Quantum fluids may also be made of photons in nonlinear media, like exciton polaritons that result from the strong coupling between cavity photons and excitons (bound electron-hole pairs in a semiconductor layer). The precise detection of the Bogoliubov dispersion in polariton quantum fluids has remained a challenging goal ever since the observation of superfluidity [10–13] and Bose Einstein condensation [14,15] therein.

In this Letter, we present a high-resolution angle-resolved coherent probe spectroscopy technique [see the setup in Fig. 1(a)] that allows for the measurement of the Bogoliubov dispersion in the linear and nonlinear regimes of interactions. In contrast to previous work [16], we continuously pump the polariton fluid near resonance to increase the spectral resolution; and unlike in photoluminescence experiments [17–21], we directly monitor the resonant response of the fluid to a coherent probe, thus efficiently isolating the signal on top of background emission from the fluid. We obtain a dramatic increase in the spectral resolution and resolve the dispersion at all wave numbers (down to $k = 0$) and reveal the soundlike behavior at low wave number. Furthermore, we show that the coherent probe may be used to generate Bogoliubov

excitations on the so-called ghost branch of the fluid, therefore opening the way to a systematic study of the quantum depletion in driven-dissipative quantum fluids [18]. Finally, we observe additional narrow spectral features, elusive so far, that go beyond the standard Bogoliubov theory of dilute gases [3,22] and stem from new, nontrivial effects due to the pump and losses [23,24].

Bogoliubov dispersion of collective excitations.—At the mean-field level, the dynamics of polaritons in planar microcavities is governed by a Gross-Pitaevskii equation modified to account for their driven-dissipative nature—the polariton fluid is a nonequilibrium system where the particle decay rate γ is compensated for by continuous pumping with the laser field E_p of frequency ω_p at normal incidence to the cavity plane ($k_p = 0$). Here, we focus on the lower polariton branch, well separated from the upper one by a polariton Rabi splitting of 5.1 meV. The polariton density $n = |\psi|^2$ is related to the incident intensity $I = |E_p|^2$ by a nonlinear relation that depends on the detuning $\delta = \omega_p - \omega_{LP}$ of the pumping laser to the $k = 0$ polariton mode [25]: optical limiting is found for $\delta < 0$ and optical bistability for $\delta > \sqrt{3}\gamma/2$.

The dispersion relation of Bogoliubov excitations in the fluid expresses the k dependence of their frequency ω_B as

$$\omega_B(k) = \pm \sqrt{\left(\frac{\hbar k^2}{2m^*} - \delta + 2gn\right)^2 - (gn)^2 - i\gamma}, \quad (1)$$

where \hbar is the reduced Planck constant, m^* is the polariton mass, and g is the polariton-polariton interaction constant [26]. The real part of Eq. (1), the dispersion curve, has two branches $\omega_{B\pm}(k)$ symmetrical around the point $k = 0$. The Bogoliubov dispersion depends on the fluid properties

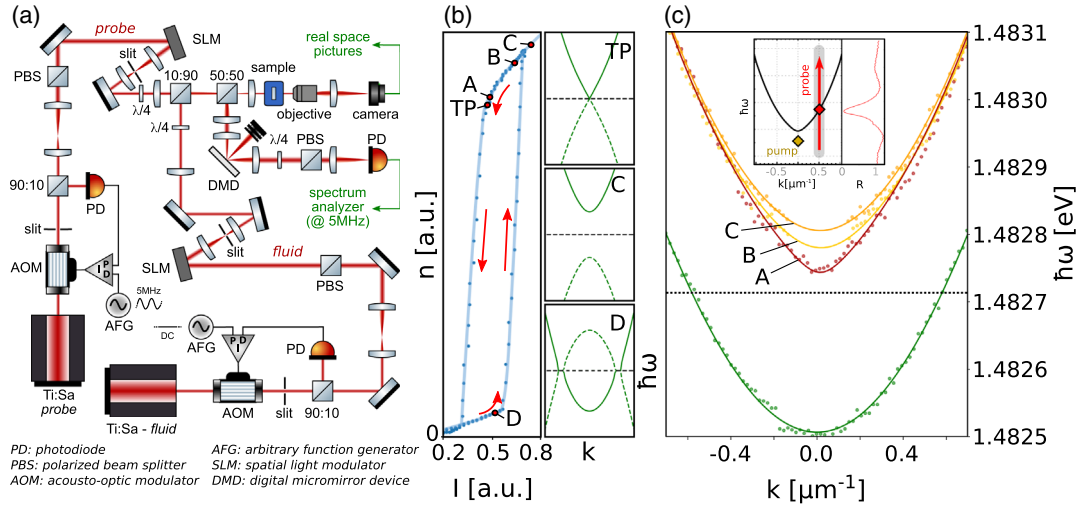


FIG. 1. Angle-resolved coherent probe spectroscopy. (a) Experimental setup. The polariton fluid is pumped at normal incidence by a Ti:sapphire laser, whose spatial mode is controlled with a SLM. The fluid is probed by another Ti:sapphire laser whose intensity is modulated by an AOM and whose angle of incidence is controlled by a second SLM. Light in the reflection port is spatially filtered with a DMD and demodulated on an electronic spectrum analyzer. (b) Optical bistability of the polariton fluid. Left: polariton density as a function of the pumping intensity. Red arrows indicate the hysteresis cycle direction. Right: theoretical dispersion for various polariton density at the turning point TP, and the points C and D along the bistability cycle. (c) Bogoliubov dispersion for a pump intensity I giving a fluid density n at working points A, B, and C along the bistability cycle. Dispersion curves are constructed by collating responses to scans of the probe frequency and wave number. Points: experimental measurements; lines, theoretical fits. Black dashed line, pump energy $\hbar\omega_p$. Green line: noninteracting polariton dispersion in the linear regime. Insets: scan example and corresponding reflectivity spectrum; orange diamond: pump frequency.

through the density n in Eq. (1), so that the shape of the dispersion curve, as well as the interaction regime, changes dramatically with detuning δ . Three examples of dispersion illustrating the main regimes are shown in Fig. 1(b). This, in turn, will impact the propagation of collective excitations in the fluid [27–30].

High resolution spectroscopy.—In order to generate a polariton fluid in a single spin state, a resonant, circularly polarized continuous-wave laser is used, and a second laser with the same polarization is then used to excite the Bogoliubov modes. Its incidence angle k_{pr} may be tuned at will and its frequency ω_{pr} can be scanned continuously over a wide range while monitoring its reflectivity. The response of the system is enhanced when the probe is resonant with a collective excitation $\omega_{pr}(k_{pr}) = \omega_B(k_{pr})$, inducing a drop (peak) in the cavity’s reflectivity (transmittivity). The spectral position of the reflectivity dips as a function of k_{pr} directly gives the Bogoliubov dispersion. In terms of many-body theory, the coherent probe beam couples to the polariton field component at k_{pr} and the system response is read out on the polariton field, therefore this method provides a direct measurement of the impulse response (i.e., the Green’s function) of the polariton field.

Experimentally, at the output of the cavity, the signal drops (peaks) are dwarfed by the intense bath of photons stemming from the fluid beam. To counter this, we modulate the probe’s amplitude with an acousto-optic modulator (AOM) operating at a frequency f_{mod}

significantly higher than the spectral width of the fluid laser. Light coming out of the cavity is focused on a photodiode connected to an electronic spectrum analyzer that demodulates at f_{mod} , thus separating the signal from the background fluid. Meanwhile, the angular resolution of the detection system is precisely controlled by means of a digital micromirror device (DMD) positioned in the Fourier plane of the cavity.

Experimental implementation.—The setup is shown in Fig. 1(a). The sample is a semiconductor microcavity made of two highly reflecting planar GaAs/AlGaAs Bragg mirrors, within which three InGaAs quantum wells separated by a substrate made of GaAs are placed at the three antinodes of the field. The cavity finesse is on the order of 3000. The polariton mass within is $m^* = 6.0 \times 10^{-35}$ kg. The experiments are performed in an open-flow helium cryostat ($T = 4$ K). The polariton fluid is pumped with a collimated, continuous-wave Ti:sapphire laser (linewidth less than 1 MHz) that illuminates the cavity at normal incidence, creating a spot of diameter $100 \mu\text{m}$. The transverse intensity profile of the fluid beam is controlled with a spatial light modulator (SLM), and operation is done with either a Gaussian or a top-hat mode. The coherent probe is another continuous-wave Ti:sapphire laser whose Gaussian spot has a $50 \mu\text{m}$ waist and whose amplitude is modulated by an AOM at $f_{\text{mod}} = 5$ MHz. The frequency of the probe is continuously scanned over a range of 120 GHz (~ 0.5 meV) around the fluid’s frequency ω_p . The angle

of incidence of the probe field on the cavity is controlled with a second SLM.

Here we present reflectivity data. As shown in Fig. 1(a), the reflected light is separated from incoming light by a 50/50 beam splitter placed before the cryostat. In the detection arm, the DMD is used as a k -tunable circular pinhole of controllable position and diameter. Placed in the reciprocal space of the cavity plane, it selects the reflected light at the wave number k on which the displayed pinhole is centered. When the pinhole and the probe are at the same k , four-wave mixing emission that may appear at $-k$ is cut off. As for the spectral resolution of the measurements, our technique does not rely on an optical spectrometer, and it is only limited by the spectral width of the probe laser, here narrower than 250 kHz (< 1 neV), while the angular resolution is given by the diameter of pinholes displayed on the DMD, here $\delta k = 0.0189 \pm 0.0005 \mu\text{m}^{-1}$.

Shape of the dispersion curve.—Since we create the polariton fluid with near-resonant pumping, we are able to study the shape of the dispersion curve as a function of the detuning δ and the pump intensity I . In order to operate in the bistable regime, one must have $\omega_p > \omega_{LP}$, such that $\delta > \sqrt{3}\gamma/2$. We can reach the hysteresis region of the bistable loop by increasing I above the bistability threshold and then decreasing it back until the turning point. This procedure must be repeated each time δ is modified. Below, we first present the results for $\delta = 0.2$ meV.

Figures 1(b) and 1(c) show the bistability curve of the polariton fluid and typical dispersion curves $\omega_{B+}(k)$ corresponding to working points A, B, and C. The insets in Fig. 1(c) show a scan of the coherent probe frequency ω_{pr} at a given k_{pr} and the response in the cavity's reflectivity—when $\omega_{pr}(k_{pr}) = \omega_B(k_{pr})$, a dip centered at the energy of the resonance is observed in the reflectivity. The dispersion is reconstructed by collating these scans (separated by $\delta k = 0.019 \mu\text{m}^{-1}$) and tracking the minima of the dips at each k_{pr} , represented by the dots in Fig. 1(c). Here the fluid is pumped with a Gaussian mode and the solid lines in Fig. 1(c) are the moving average over 5 experimental points, $\omega_{B+}(k)$.

As expected from the theory [26], there is a gap between the pump energy (horizontal black dashed line) and the minimum of the $\omega_{B+}(k)$ branch at $k = 0$. Even though the size of the gap decreases when the pump intensity is decreased from working point C to A, it is still present at working point A near the turning point of the bistability. Although the density distribution of the fluid is steepened by the bistable behavior of the system, creating the polariton fluid with a Gaussian spatial mode does yield a nonuniform density [17], from which the dispersive properties of the fluid depend on space. In other words, the dispersion curves shown in Fig. 1(c) result from a spatial average over the different dispersion relations across the probe spot. Nonetheless, at low energy the behavior

deviates from the pure parabolic shape, which is a hint of collective effects due to phononic interactions. Still, spatial resolution is required to probe the fluid with a fixed local density.

In order to observe the closing of the gap between $\omega_{B+}(k)$ and ω_p , the region of spatial integration has to be reduced so as to measure the dispersion for a specific value of the local density n . To this end, the probe intensity profile is reshaped with the SLM into a narrow ring. The radius of the ring is chosen to match the outer edge of the fluid, where the local fluid density is as close as possible to the turning point of the bistability cycle ($\delta = gn$). In Fig. 2(a), we present the coherent probe reflectivity spectra in this configuration. The small red dots show the position of the dip minimum for each frequency scan. We observe the closing of the energy gap and we evidence directly, without any data processing, that $\omega_{B+}(k)$ is linear at low wave number (white dashed line) and parabolic at large wave number. The agreement with numerical simulations based on a driven-dissipative version of the GPE [24] [bottom row of Fig. 2(a)] is excellent.

The speed of sound in the fluid is precisely obtained from the linear slope at low energy: $c_s = 0.54 \mu\text{m ps}^{-1}$. Interestingly, this value is reduced by a factor α with respect to the theoretical prediction $c_s^{th} = \sqrt{\delta/m_{LP}}$. This can be explained in terms of an incoherent reservoir of long-lived dark excitons providing an additional contribution to the blueshift and to the bistability curve but not to the speed of sound [17,19,20,24]. In our experiment, an estimate of the reservoir contribution to the blueshift $g_r n_r = 0.75 \delta$ is obtained from the measured values of $\alpha \simeq 0.49$ and of the total blueshift $gn + g_r n_r = \delta$ at the turning point of the bistability.

Detection of the ghost branch.—The discussion so far has focused on $\omega_{B+}(k)$, the positive frequency solution of the dispersion relation (1), i.e., resonant excitations above the ground state. Since we excite the system with a coherent probe coupled to the polariton field (and not with a time-dependent external potential as in standard Bragg spectroscopy of ultracold atomic gases [31]), our method also enables the observation of the negative-energy solution ω_{B-} that is often referred to as the “ghost branch.” Unlike the ω_{B+} branch, the ghost branch does not resonate with the cavity, and is spontaneously populated by quantum depletion of the fluid, which is weak. This renders its direct observation in photoluminescence difficult [17–19]. Here, we stimulate the coherent conversion of the fluid of polaritons toward the ghost branch via the coherent probe [32]: this configuration induces a four-wave mixing (FWM) process $(\omega_p, \omega_p) \rightarrow (\omega_+, \omega_-)$, and the probe at $\omega_- < \omega_p$ directly seeds Bogoliubov excitations on the ghost branch which manifest as an amplification peak $R > 1$ above the baseline of the probe's reflectivity spectrum.

Within the Bogoliubov theory, this FWM process consists in the mixing of creation and destruction operators of

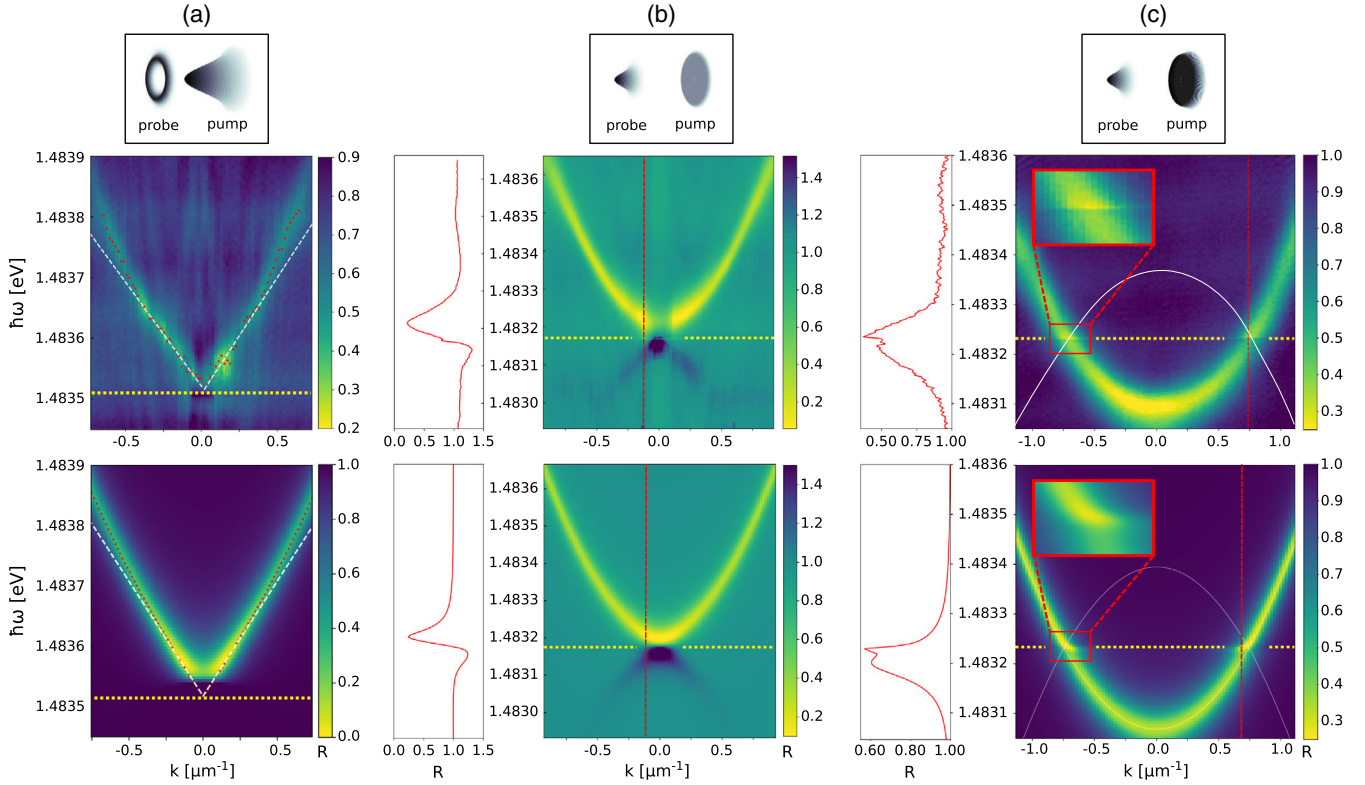


FIG. 2. Dispersion of collective excitations. Top row: spatial mode profile of the pump and coherent probe lasers. The peak probe intensity is always 1% of the pump (peak) intensity. The top-hat intensity (b) [(c)] is 50% (70%) of the Gaussian peak intensity (a). Middle row: collated probe reflectivity scans separated by $\delta k = 0.019 \mu\text{m}^{-1}$. Bottom row: corresponding numerical simulations. Vertical red-dashed lines: k slice corresponding to the energy scan shown on the left panel. Horizontal yellow dotted line: fluid pumping laser energy $\hbar\omega_p$. (a) Sonic dispersion. Density at turning point A of the bistability loop, with $\delta = gn + g_r n_r$. White dashed line: linear dispersion fit of the speed of sound. (b) Ghost branch. Density near the turning point A of the bistability loop. The ghost branch is coherently seeded by the probe and is visible at $\omega < \omega_p$. (c) Precursors of instabilities. Low density regime. Plateaus are visible at $\omega = \omega_p$ around $k = \pm 0.74 \mu\text{m}^{-1}$ leading to the Fano features visible in the inset. White curve, position of the ghost branch. R is normalized to 1 for the off-resonance reflected probe intensity.

the polariton field. Because of the phase matching condition, this mixing is only sizable within a limited wave vector region, so efficient angular selectivity is crucial. In addition, by using a top-hat intensity profile we create a fluid of homogeneous density. As a result, the FWM process takes place in a reduced range of interaction energies, thus optimizing the population of the ghost branch and its detection. In Fig. 2(b), the fluid is pumped with an intensity as close as possible to the turning point of the bistability, where the FWM is most efficient [26]. Both branches of the dispersion relation at $\omega_{B\pm}$ are clearly visible, in good agreement with the numerical simulations shown in the bottom row of Fig. 2(b) and the strength of the ghost branch decreases rapidly with k , similarly to the behavior observed in cold atoms [33–35].

Fluid instabilities.—Because of the driven-dissipative nature of polaritons, the quantum fluid is intrinsically out of equilibrium. This explains the gap that opens between the dispersion curve and the pump energy in the nonlinear regime of interactions [cf. Fig. 1(c)], a marked departure from the standard Bogoliubov theory of dilute gases.

Even more interestingly, out-of-equilibrium physics is at the origin of dynamical instabilities of the fluid. When operating in a regime of weak interactions ($\delta > 3gn$) corresponding to working point D in Fig. 1(b), the $\omega_{B\pm}$ branches cross around $k = \pm 0.74 \mu\text{m}^{-1}$ and $\omega = \omega_p$, and stick together for $\delta - 3gn < (\hbar k^2/2m^*) < \delta - gn$ [36,37], as in Fig. 2(c). There, the sign inside the square root in Eq. (1) becomes negative: the real parts $\text{Re}(\omega_B)$ both stay at $\omega = \omega_p$, yielding plateaus in the dispersion curve [see also Fig. 1(b)], while the imaginary parts $\text{Im}(\omega_B)$ are split but remain both negative under the effect of dissipation. The narrow features in the reflectivity visible in the insets are associated to the Fano-like interference corresponding to the smaller imaginary-part pole. This is an important marked departure from the physics of dilute gases. Although, in our experiment in Fig. 2(c) the pump intensity is kept low enough for the fluid to remain dynamically stable, our high-resolution spectroscopy method reveals the observation of this out-of-equilibrium feature for the first time. For slightly higher pump intensity, these plateaus would lead to dynamical instabilities predicted in [23] so

our method is well suited for the in-depth analysis of this instability as well as other turbulent dynamics, such as snake instabilities [38] or quantum turbulence [39–43].

Conclusion.—We have presented an angle-resolved coherent probe spectroscopy method to measure the dispersion of collective excitations in a quantum fluid of exciton polaritons within a semiconductor microcavity. The high energy- and wave-number-resolution of our spectroscopy method enables the accurate study of the Bogoliubov dispersion in all regimes of interactions [44], from the parabolic dispersion of high-energy single-particle excitations to the sonic dispersion of long-wavelength collective excitations. Moreover our method allows for the excitation of the negative-norm ghost branch, suggesting that quantum depletion is present in our system, thus calling for a quantitative study of this effect. Finally, we have observed the influence of the polariton fluid local density on the dispersion at low wave number and evidenced the presence of a dark excitonic reservoir that modifies the effective speed of sound in the fluid. This calls for a quantitative spectroscopic study of the reservoir. The versatility of our method is further illustrated by the resolution of narrow spectral features that specifically stem from nonequilibrium effects such as the controlled opening of an energy gap and the appearance of horizontal plateaus precursory of dynamical instabilities. Our method will be an essential tool to quantitatively characterize the polariton-polariton and polariton-reservoir interactions in different regimes, and to address the nonequilibrium physics of Goldstone modes induced by spontaneous phase symmetry breaking [46] and for the study of quantum amplification effects such as Hawking radiation or rotational superradiance in analog gravity scenarios like (rotating) black holes [30,47,48].

We acknowledge financial support from the H2020-FETFLAG-2018-2020 project “PhoQuS” (n.820392). I. C. acknowledges financial support from the Provincia Autonoma di Trento and from the Q@TN initiative. Q. G. and A. B. are members of the Institut Universitaire de France.

[1] F. London, *Nature (London)* **141** (1938).
 [2] L. Landau, *Phys. Rev.* **60**, 356 (1941).
 [3] N. N. Bogolyubov, *J. Phys. USSR* **11**, 23 (1947).
 [4] R. P. Feynman, *Phys. Rev.* **94**, 262 (1954).
 [5] P. Szriftgiser, D. Guery-Odelin, M. Arndt, and J. Dalibard, *Phys. Rev. Lett.* **77**, 4 (1996).
 [6] M.-O. Mewes, M. R. Andrews, N. J. van Druten, D. M. Kurn, D. S. Durfee, C. G. Townsend, and W. Ketterle, *Phys. Rev. Lett.* **77**, 988 (1996).
 [7] R. Onofrio, C. Raman, J. M. Vogels, J. R. Abo-Shaeer, A. P. Chikkatur, and W. Ketterle, *Phys. Rev. Lett.* **85**, 2228 (2000), publisher: American Physical Society.
 [8] Q. Fontaine, T. Bienaimé, S. Pigeon, E. Giacobino, A. Bramati, and Q. Glorieux, *Phys. Rev. Lett.* **121**, 183604 (2018).

[9] C. Piekarski, W. Liu, J. Steinhauer, E. Giacobino, A. Bramati, and Q. Glorieux, *Phys. Rev. Lett.* **127**, 023401 (2021).
 [10] K. G. Lagoudakis, M. Wouters, M. Richard, A. Baas, I. Carusotto, R. André, L. S. Dang, and B. Deveaud-Plédran, *Nat. Phys.* **4**, 706 (2008).
 [11] S. Utsunomiya, L. Tian, G. Roumpos, C. W. Lai, N. Kumada, T. Fujisawa, M. Kuwata-Gonokami, A. Löffler, S. Höfling, A. Forchel, and Y. Yamamoto, *Nat. Phys.* **4**, 700 (2008).
 [12] A. Amo, J. Lefrère, S. Pigeon, C. Adrados, C. Ciuti, I. Carusotto, R. Houdré, E. Giacobino, and A. Bramati, *Nat. Phys.* **5**, 805 (2009).
 [13] V. Kohnle, Y. Léger, M. Wouters, M. Richard, M. T. Portella-Oberli, and B. Deveaud-Plédran, *Phys. Rev. Lett.* **106**, 255302 (2011).
 [14] J. Kasprzak, M. Richard, S. Kundermann, A. Baas, P. Jeambrun, J. M. J. Keeling, F. M. Marchetti, M. H. Szymańska, R. André, J. L. Staehli *et al.*, *Nature (London)* **443**, 409 (2006).
 [15] R. Balili, V. Hartwell, D. Snoke, L. Pfeiffer, and K. West, *Science* **316**, 1007 (2007).
 [16] V. Kohnle, Y. Léger, M. Wouters, M. Richard, M. T. Portella-Oberli, and B. Deveaud, *Phys. Rev. B* **86**, 064508 (2012).
 [17] P. Stepanov, I. Amelio, J.-G. Rousset, J. Bloch, A. Lemaître, A. Amo, A. Minguzzi, I. Carusotto, and M. Richard, *Nat. Commun.* **10**, 3869 (2019).
 [18] M. Pieczarka, E. Estrecho, M. Boozarjmehr, O. Bleu, M. Steger, K. West, L. N. Pfeiffer, D. W. Snoke, J. Levinsen, M. M. Parish *et al.*, *Nat. Commun.* **11**, 429 (2020).
 [19] M. Pieczarka, O. Bleu, E. Estrecho, M. Wurdack, M. Steger, D. W. Snoke, K. West, L. N. Pfeiffer, A. G. Truscott, E. A. Ostrovskaya *et al.*, *Phys. Rev. B* **105**, 224515 (2022).
 [20] E. Estrecho, M. Pieczarka, M. Wurdack, M. Steger, K. West, L. N. Pfeiffer, D. W. Snoke, A. G. Truscott, and E. A. Ostrovskaya, *Phys. Rev. Lett.* **126**, 075301 (2021).
 [21] D. Biegańska, M. Pieczarka, E. Estrecho, M. Steger, D. W. Snoke, K. West, L. N. Pfeiffer, M. Syperek, A. G. Truscott, and E. A. Ostrovskaya, *Phys. Rev. Lett.* **127**, 185301 (2021).
 [22] L. P. Pitaevskij and S. Stringari, *Bose-Einstein Condensation and Superfluidity*, International Series of Monographs on Physics Vol. 164 (Oxford University Press, Oxford, 2016), reprinted (with corrections) ed., ISBN 978-0-19-875888-4.
 [23] C. Ciuti and I. Carusotto, *Phys. Status Solidi (b)* **242**, 2224 (2005).
 [24] I. Amelio, A. Minguzzi, M. Richard, and I. Carusotto, *Phys. Rev. Research* **2**, 023158 (2020).
 [25] A. Baas, J. P. Karr, H. Eleuch, and E. Giacobino, *Phys. Rev. A* **69**, 023809 (2004).
 [26] I. Carusotto and C. Ciuti, *Rev. Mod. Phys.* **85**, 299 (2013).
 [27] A. Maître, G. Lerario, A. Medeiros, F. Claude, Q. Glorieux, E. Giacobino, S. Pigeon, and A. Bramati, *Phys. Rev. X* **10**, 041028 (2020).
 [28] G. Lerario, A. Maître, R. Boddada, Q. Glorieux, E. Giacobino, S. Pigeon, and A. Bramati, *Phys. Rev. Research* **2**, 023049 (2020).

- [29] G. Lerario, S. V. Koniakhin, A. Maître, D. Solnyshkov, A. Zilio, Q. Glorieux, G. Malpuech, E. Giacobino, S. Pigeon, and A. Bramati, *Phys. Rev. Research* **2**, 042041(R) (2020).
- [30] M. J. Jacquet, L. Giacomelli, Q. Valnais, M. Joly, F. Claude, E. Giacobino, Q. Glorieux, I. Carusotto, and A. Bramati, [arXiv:2110.14452](https://arxiv.org/abs/2110.14452).
- [31] J. Stenger, S. Inouye, A. P. Chikkatur, D. M. Stamper-Kurn, D. E. Pritchard, and W. Ketterle, *Phys. Rev. Lett.* **82**, 4569 (1999).
- [32] J. M. Zajac and W. Langbein, *Phys. Rev. B* **92**, 165305 (2015).
- [33] R. Lopes, C. Eigen, N. Navon, D. Clément, R. P. Smith, and Z. Hadzibabic, *Phys. Rev. Lett.* **119**, 190404 (2017).
- [34] H. Cayla, S. Butera, C. Carcy, A. Tenart, G. Hercé, M. Mancini, A. Aspect, I. Carusotto, and D. Clément, *Phys. Rev. Lett.* **125**, 165301 (2020).
- [35] A. Tenart, G. Hercé, J.-P. Bureik, A. Dureau, and D. Clément, *Nat. Phys.* **17**, 1364 (2021).
- [36] C. Ciuti, P. Schwendimann, and A. Quattropani, *Phys. Rev. B* **63**, 041303(R) (2001).
- [37] P. G. Savvidis, C. Ciuti, J. J. Baumberg, D. M. Whittaker, M. S. Skolnick, and J. S. Roberts, *Phys. Rev. B* **64**, 075311 (2001).
- [38] F. Claude, S. V. Koniakhin, S. V. Koniakhin, A. Maître, S. Pigeon, G. Lerario, D. D. Stupin, Q. Glorieux, Q. Glorieux, E. Giacobino, and A. Bramati, *Optica* **7**, 1660 (2020).
- [39] L. Madeira, A. Cidrim, M. Hemmerling, M. A. Caracanhas, F. E. A. dos Santos, and V. S. Bagnato, *AVS Quantum Sci.* **2**, 035901 (2020).
- [40] S. V. Koniakhin, O. Bleu, G. Malpuech, and D. D. Solnyshkov, *Chaos, Solitons Fractals* **132**, 109574 (2020).
- [41] L. Galantucci, A. W. Baggaley, C. F. Barenghi, and G. Krstulovic, *Eur. Phys. J. Plus* **135**, 547 (2020).
- [42] S. V. Koniakhin, G. Malpuech, D. Solnyshkov, and A. V. Nalitov, *Europhys. Lett.* **133**, 66001 (2021).
- [43] L. Giacomelli and I. Carusotto, [arXiv:2110.10588](https://arxiv.org/abs/2110.10588).
- [44] Extraction of the Tan contact in polariton fluids is often made difficult by their nonequilibrium dynamics, which hinders a direct application of the fluctuation-dissipation theorem. Such a limitation may be alleviated in nonresonantly pumped, long-lifetime condensates that are closer to thermal equilibrium [45].
- [45] A. Chiocchetta, A. Gambassi, and I. Carusotto, *Universal Themes of Bose-Einstein Condensation* (Cambridge University Press, Cambridge, 2017).
- [46] M. Wouters and I. Carusotto, *Phys. Rev. A* **76**, 043807 (2007).
- [47] H. S. Nguyen, D. Gerace, I. Carusotto, D. Sanvitto, E. Galopin, A. Lemaître, I. Sagnes, J. Bloch, and A. Amo, *Phys. Rev. Lett.* **114**, 036402 (2015).
- [48] M. J. Jacquet, T. Boulier, F. Claude, A. Maître, E. Cancellieri, C. Adrados, A. Amo, S. Pigeon, Q. Glorieux, A. Bramati, and E. Giacobino, *Phil. Trans. R. Soc. A* **378**, 20190225 (2020).